JOURNAL OF Materials CHEMISTRY

Synthesis, characterization and comparative study of the electrochemical properties of doped lithium manganese spinels as cathodes for high voltage lithium batteries

L. Hernán,[a] J. Morales,*[a] L. Sánchez,[a] E. Rodríguez Castellón[b] and M. A. G. Aranda[b]

[a]*Departamento de Química Inorgánica, Facultad de Ciencias, Campus de Rabanales, Edificio C-3, Universidad de Córdoba, Córdoba, Spain. E-mail: iq1mopaj@uco.es*
[b]*Departamento de Química Inorgánica, Facultad de Ciencias, Campus de Teatinos, Universidad de Málaga, Málaga, Spain*

Received 24th October 2001, Accepted 12th December 2001
First published as an Advance Article on the web 6th February 2002

Three series of spinels of nominal composition $LiM_xMn_{2-x}O_4$ (M = Fe, Co, Ni; $x \approx 0.3$) were prepared by using a carbonate-based precursor method followed by calcining in the air at 400, 600 and 900 °C. The spinels were characterized by chemical analysis, X-ray diffraction (XRD) and X-ray photoelectron spectroscopy (XPS), and tested as cathodes in lithium cells over the range 3.5 to 5.2 V *vs* Li/Li^+. XPS data revealed that Co and Fe adopt a tervalent oxidation state whereas Ni is in a divalent state. No sign of Mn^{2+} was detected. Above 400 °C, all the spinels contain a small fraction of a transition element in their 8a tetrahedral sites, together with lithium ions. The three series have the ability to extract lithium above 4.5 V, which is accompanied by the oxidation of the dopant transition metal. The reversibility of this reaction increases with higher calcining temperatures as a result of better crystallinity and the smoother particle surfaces. However, the iron spinels depart from this trend; thus, the cell obtained from the sample heated at 600 °C possesses good cycling properties and maintains a capacity of *ca.* 100 A h kg^{-1} upon cycling. By contrast, the Fe-containing spinel obtained at 900 °C loses its whole capacity after the first few cycles. Partial extrusion of iron as Fe_2O_3 and non-uniformity in particle size and shape may account for its poor electrochemical behavior. The Co- and Ni-containing spinels obtained at 900 °C lack these features; their cells exhibit excellent capacity retention upon extended cycling and are capable of delivering 100 and 120 A h kg^{-1}, respectively, at an average voltage of 4.5 V. They can supply a higher energy density than the common spinel $LiMn_2O_4$.

Introduction

Ever since Dahn *et al.*[1] demonstrated the ability of inverse spinels, $LiMVO_4$ (M = Ni, Co), to yield voltages as high as 4.8 V upon electrochemical removal of lithium, this new generation of intercalation electrodes has aroused increasing interest as it provides the means for manufacturing Li-ion cells of higher voltages than those commercially available based on $LiCoO_2$ and $LiMn_2O_4$ electrodes. Unfortunately, a serious problem remains with inverse spinels: their capacity fades considerably after a few cycles, which has been ascribed to oxidation of the electrolyte at such high voltages.

Sigala *et al.*[2] were the first to envisage 5 V alternative materials such as $LiCr_xMn_{2-x}O_4$, also based on the spinel framework. These chromium-substituted spinels also exhibit poor cycling performance and the origin of the high voltage step of about 4.9 V is a redox reaction (the oxidation of Cr^{3+} to Cr^{4+}).[3] This process has been exploited in other Li–Mn spinels substituted with V, Fe, Co, Ni and Cu, which also exhibit an operating voltage close to 5 V after reaching the 4 V plateau.[4-10] Good cycling properties have been found in Ni- and Cu-based spinels;[7,8] however, some cell capacity is sacrificed owing to the increase in the Mn average oxidation state resulting from the accommodation of Ni^{2+} and Cu^{2+} in the spinel framework. By contrast, substitution of Mn by tervalent cations such as Cr^{3+}, Fe^{3+} and Co^{3+} has yielded disappointing results in cycling properties, though the cell capacity should hardly be affected.[3,6,11] So far, most work on this topic has focused on the study of individual systems and the conclusions reported are often difficult to generalize because the electrochemical performance of the cell can be significantly affected by a number of factors including the experimental synthetic conditions.

In this paper, we report a comparative study of doped Li–M–Mn–O (M = Fe, Co, Ni) spinel oxides acting as cathodes in lithium cells operating at high voltages (3.5–5.2 V). We used a based-carbonate precursor method, which is highly effective for the preparation of spinels that exhibit excellent cycling performance in lithium cells over the potential window 3.3–2.3 V.[12,13] These doped spinels were prepared from identical metal ratios for the three systems in order to obtain mixed oxides of similar cation content and used the calcining temperature as variable. Differences in electrochemical behavior were characterized in terms of stoichiometry and of textural, structural and electronic properties.

Experimental

$LiM_xMn_{2-x}O_4$ (M = Fe, Co, Ni) cathode materials were prepared by using a precursor method based on the formation of mixed carbonates involving the addition of a 1 M solution of $NaHCO_3$ to a 0.5 M solution of the divalents ions Mn(II) and M(II) under a continuous CO_2 stream. The respective precursors were prepared in an M/Mn ratio of 0.17 and the precipitates filtered off, dried, thoroughly mixed with appropriate amounts of LiOH (Li/Mn+M atomic ratio 0.5) and calcined at 400, 600 and 900 °C in the air for 24 h. Hereafter, we label the samples by the symbol for the dopant transition metal, followed by the heating temperature. The elemental composition of the final products was determined by atomic absorption spectrometry. The average oxidation state of the

 DOI: 10.1039/b109717m

metal ions was measured as follows: about 20 mg of sample were dissolved in 40 ml of 0.1 M Fe^{2+} in 0.01 M H_2SO_4 under a continuous flow of argon. The solution was titrated with a 0.01 M $KMnO_4$ solution previously standardized with $Na_2C_2O_4$. Titrant consumption was assigned to excess Fe^{2+} ions in the sample solution and used to calculate the oxygen-to-metal ratios.

X-ray diffraction patterns (XRD) were recorded at room temperature on a Siemens D5000 X-ray diffractometer, using non-monochromated Cu Kα radiation (wavelength: 1.5405 and 1.5443 Å for Kα_1 and Kα_2, respectively) and a graphite monochromator for the diffracted beam. The scan conditions for structural refinement were 15–90° (2θ) which included 15 (*hkl*) planes, a 0.02° step size and 5 s per step. X-ray photoelectron spectra (XPS) were obtained on a Physical Electronics PHI 5700 spectrometer using non-monochromated Mg Kα radiation. High-resolution spectra were recorded at a 45° take-off-angle by using a concentric hemispherical analyzer operating in the constant pass energy mode at 29.35 eV, and an analysis area 720 μm in diameter. Under these conditions, the Au $4f_{7/2}$ line was recorded with 1.16 eV FWHM at a binding energy of 84.0 eV. The spectrometer energy scale was calibrated by using the Cu $2p_{3/2}$, Ag $3d_{5/2}$ and Au $4f_{7/2}$ photoelectron lines at 932.7, 368.3 and 84.0 eV, respectively. Charge referencing was measured against adventitious carbon (C 1s 284.8 eV). Samples were mounted on a holder without adhesive tape and kept under high vacuum in the preparation chamber overnight before they were transferred to the analysis chamber of the spectrometer. Each region was scanned several times to have a good signal-to-noise ratio. Survey spectra over the range 0–1200 eV were recorded at a 187.85 eV pass energy. The pressure in the analysis chamber was maintained below 5×10^{-6} Pa. The PHI ACCESS ESCA-V6.0 F software package was used for acquisition and processing of data. A Shirley-type background was subtracted from the signals. Recorded spectra were always fitted using Gauss-Lorentz curves in order to more accurately determine the binding energy of the different element core levels. Scanning electron microscopy (SEM) images were obtained on a Jeol JMS 6400 microscope.

Electrochemical experiments were carried out by using two Swagelock-type electrode cells with lithium as counter and reference electrode. Powdered spinel pellets (7 mm diameter) were prepared by pressing, in a stainless steel grid, *ca.* 4 mg of active material with graphite (7.5% wt), acetylene black (7.5% wt) and PTFE (5% wt). The electrolyte was 1 M anhydrous $LiPF_6$ (supplied by Strem Chem.) in a 1 : 2 mixture of ethylene carbonate (EC) and diethyl carbonate (DEC) (both supplied by Merck). Cells were assembled under an argon atmosphere in an M-Braun glove-box with a moisture content lower than 3 ppm. Cells were cycled at a 0.25 mA cm^{-2} current density that was controlled *via* a Macpile II potentiostat-galvanostat. In order to ensure reproducibility in the measurements, all electrochemical measurements were repeated at least twice.

Results and discussion

Structural characterization

All calcined precursors crystallize in the spinel structure as the main phase. However, the heating temperature introduced subtle differences as revealed by XRD (Fig. 1). Thus, at 400 °C, diffraction peaks were weak and broad, which suggest poor crystallinity of particles. At higher temperatures, peaks were more intense and sharper. Also, new peaks that could not be indexed in a cubic spinel phase became apparent, particularly at 900 °C, that suggested the presence of small amounts of impurities. For the Co-substituted compound, two additional peaks at 7.07 and 5.63 Å were detected likely due to an unknown impurity. The pattern for the Ni-substituted compound has three extra peaks at 5.63, 2.07 and 1.46 Å. The

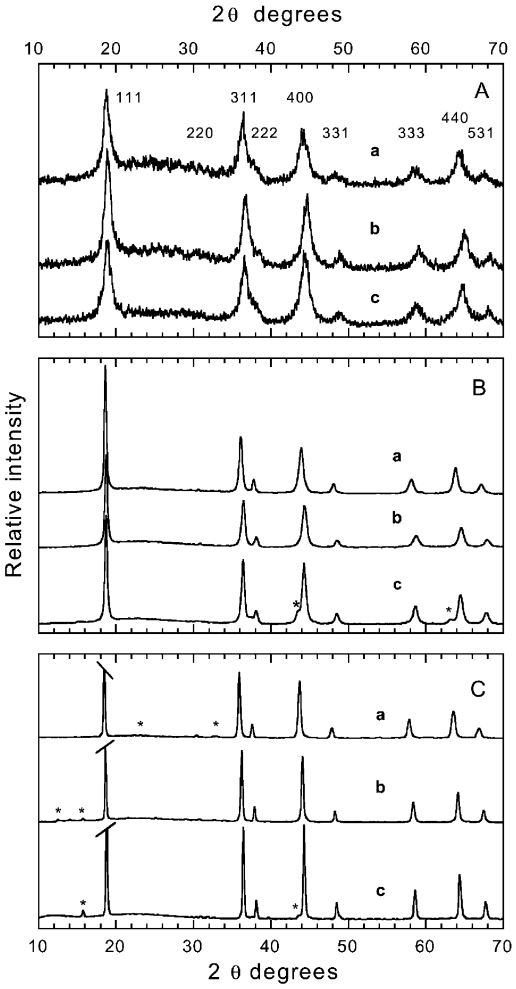

Fig. 1 XRD patterns for the Li–M–Mn–O (M = Fe, Co, Ni) spinel oxides; (a) Fe, (b) Co and (c) Ni. Calcining temperature: (A) 400; (B) 600, (C) 900 °C. Asterisks denote impurities.

interplanar spacing of the last two peaks agrees fairly well with those reported for $Li_xNi_{1-x}O$. This impurity has also been detected in a spinel of nominal composition $LiNi_{0.5}Mn_{1.5}O_4$ prepared by a sol–gel process.[7] The XRD pattern for the Fe-substituted spinel suggests the presence of a small amount of α-Fe_2O_3 at 900 °C.

This synthetic method yields particles of rather uniform size distribution, as shown by the scanning electron micrographs of Figs. 2A and B. Particle size ranges from 2 to 4 μm and remains

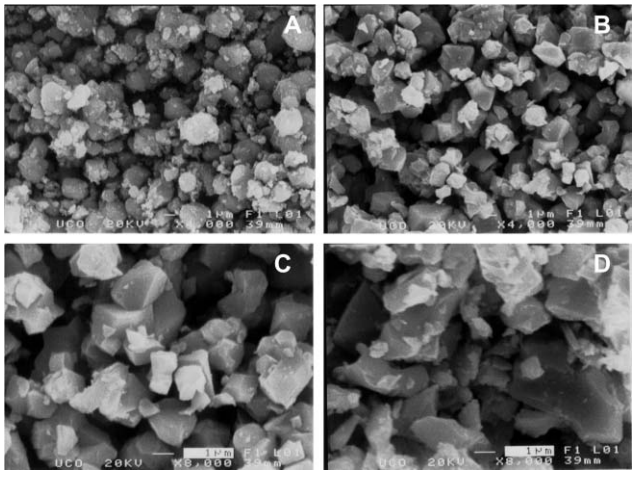

Fig. 2 Scanning electron micrographs for (A) Co 400, (B) Co 600, (C) Ni 900 and (D) Fe 900.

Table 1 Composition and average Mn oxidation state (Z_{Mn}) for Li–M–Mn–O spinels

T/°C	Sample	O/(Li+M+Mn)	Z_{Mn}
400	$Li_{0.90}Fe_{0.30}Mn_{1.72}O_4$	1.36	3.61
	$Li_{0.83}Co_{0.29}Mn_{1.67}O_4$	1.43	3.76
	$Li_{0.96}Ni_{0.33}Mn_{1.72}O_4$	1.33	3.71
600	$Li_{0.92}Fe_{0.32}Mn_{1.80}O_4$	1.31	3.40
	$Li_{0.97}Co_{0.30}Mn_{1.70}O_4$	1.34	3.60
	$Li_{0.90}Ni_{0.32}Mn_{1.66}O_4$	1.38	3.89
900	$Li_{1.02}Fe_{0.34}Mn_{1.89}O_4$	1.24	3.20
	$Li_{0.89}Co_{0.31}Mn_{1.77}O_4$	1.34	3.47
	$Li_{0.90}Ni_{0.34}Mn_{1.79}O_4$	1.32	3.54

virtually unchanged on heating. However, the particle shape of Co- and Ni-doped spinels undergoes more pronounced changes (to *pseudo* octahedral forms on heating, Fig. 2C). This reflects the above-mentioned improved crystallinity. The Fe-doped spinel behaves somewhat differently and particles adopt more uneven sizes and shapes, even at 900 °C (see Fig. 2D).

Table 1 shows the composition obtained by using a combination of atomic absorption spectroscopy and energy dispersive X-ray data, together with the average oxidation state of Mn. Most of the spinels have an O/M ratio close to 1.33, the value for a stoichiometric spinel. Three samples (*viz.* Co 400, Ni 600 and especially Fe 900) deviate from this value; the first two are cation-deficient spinels. The cation excess in the Fe 900 sample is likely due to the presence of an impurity, Fe_2O_3. The average oxidation state of Mn decreases with increasing temperature except for the Ni 600 sample (probably as a result of its Mn deficiency). As shown below, the three samples prepared at 400 °C exhibited poor electrochemical performance, and so the complementary structural and electronic study was only carried out on the other samples.

Table 2 Binding energies, in eV, of the main core level spectra for Li–M–Mn–O spinels

Sample	Li 1s	Mn $2p_{3/2}$	Fe $2p_{3/2}$	Co $2p_{3/2}$	Ni $2p_{3/2}$	O 1s
Fe 600	55.4	641.7	711.7	—	—	529.7 531.1
Fe 900	55.0	641.4	711.2	—	—	528.7 530.6 532.4
Co 600		641.5	—	779.2	—	529.0 531.0
Co 900	54.0	641.5		779.2		528.9 530.9
Ni 900		641.5	—	—	853.4	529.1 531.0

The binding energy (BE) values for the core level of the elements in the spinel compounds are shown in Table 2. The BE for Mn hardly changes through the series and the values of the Mn $2p_{3/2}$ component peak are intermediate between those reported for α-Mn_2O_3 (641.2 eV)[14] and MnO_2 (642.1 eV),[15] and larger than that for MnO (640.7 eV).[15] Moreover, the satellite peak clearly apparent for divalent manganese 5 eV above the 2 $p_{3/2}$ component[16] is absent in all the spectra. Fig. 3a compares the Mn 2p emission spectra for the Fe 600 and Fe 900 samples as an example. Therefore, Mn occurs in an oxidation state between +3 and +4, in agreement with the average oxidation state determined by titration. However, obtaining accurate information about the proportion of both ions and the changes induced on heating is beyond the resolution of XPS. In any case, the most perceptible change in the BE of Mn is that in the Fe-doped spinel, the system that undergoes the most drastic reduction in the Z_{Mn} on heating (see Table 1). The Fe 2p spectra, Fig. 3b, have a low signal-to-noise ratio, thus hindering accurate assignation of BE. Although BE for the Fe $2p_{3/2}$ emission peak seems to decrease on heating, the shake-up satellite and the Fe $2p_{1/2}$ signal remain unchanged at 718.1 and 724.2 eV, respectively. In this context, the modified Auger parameter (α*) (the sum of the binding energy of the photoelectron and the kinetic energy of the corresponding

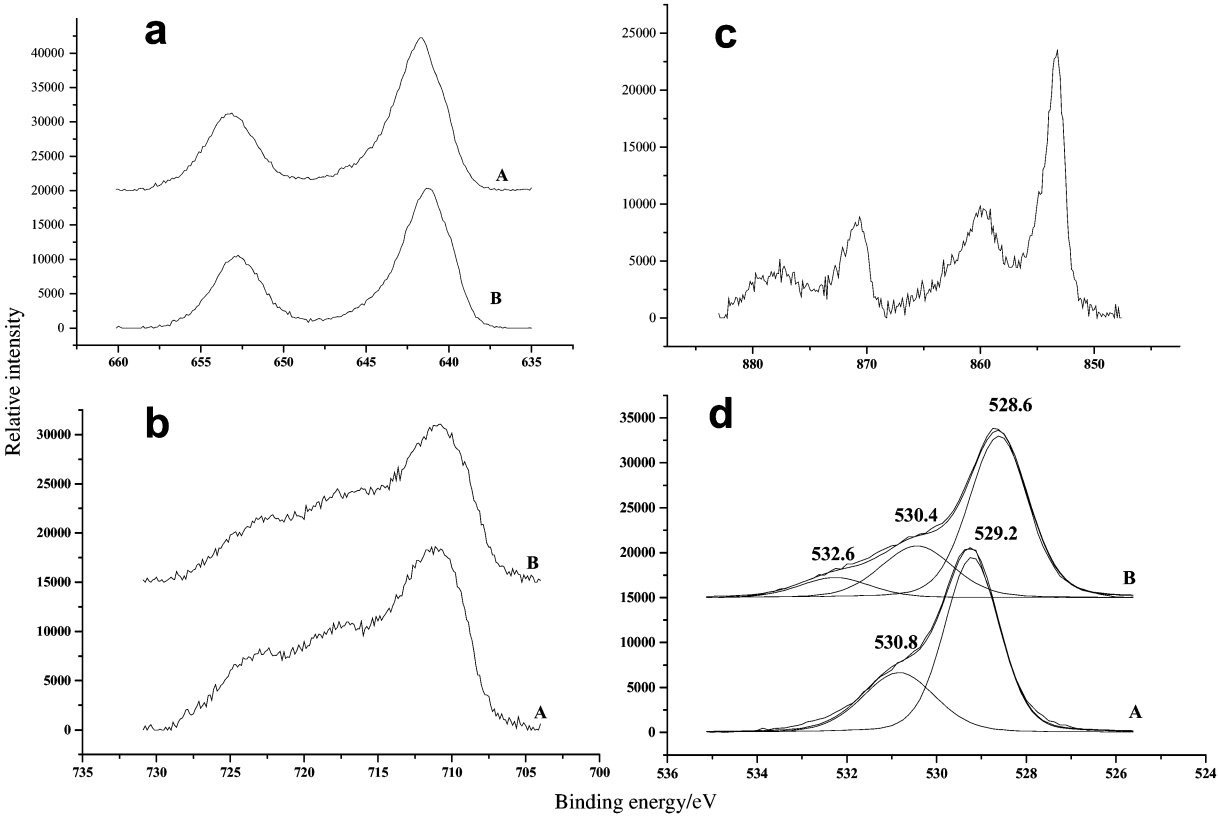

Fig. 3 (a) Mn 2p, (b) Fe 2p, (c) Ni 2p and (d) O 1s core level spectra.

Auger transition) is free from calibration errors in XPS spectra (choice of binding energy scale) and is more sensitive to chemical state than the chemical shifts in XPS.[17] The Auger peak for Fe (Fe_{LMM}) appears at 554.5 and 553.8 eV for Fe 600 and Fe 900, respectively. Thus, the difference between the calculated α^* values (1410.8 and 1411.0 eV for the Fe 600 and Fe 900 spinel, respectively) falls within experimental error. This means that the oxidation state of Fe remains virtually unchanged on heating. The BE value measured for the Fe $2p_{3/2}$ signal (particularly in the Fe 900 spinel) is somewhat higher than that reported for Fe^{3+} compounds (*viz.* Fe_2O_3 710.8–711.3 eV).[15] We addressed this problem by recording spectra with Al as excitation source. The iron spectra, whose Fe $2p_{3/2}$ component peaks appeared at 710.8 eV for both samples, are typical of Fe(III) oxides.[18] Also, the separation of the $2p_{1/2}$ and $2p_{3/2}$ spin-orbit level, 13.6 eV, and the difference between the $2p_{3/2}$ line and the satellite, 8.1 eV, are consistent with the results of Armelao *et al.*[19] for high-purity Fe_2O_3 thin films. The BE values for Co 2p remain constant, within experimental error, on heating and are close to that found for the Co_3O_4 spinel (Co $2p_{3/2}$ 779.3–779.9 eV)[15] but deviate from that reported for CoO (Co $2p_{3/2}$ 780.1–780.9 eV).[15] This result reveals that Co, like Fe, is in a tervalent oxidation state. The XPS Ni $2p_{3/2}$ spectra consist of a rather symmetric peak centered at 853.4 eV. This value is somewhat lower than that reported for other Ni-based spinels (*viz.* $NiMn_2O_4$, 855.2 eV)[15] but is close to that recently reported for $LiNi_{0.5}Mn_{1.5}O_4$ (854.04 eV).[20] Moreover, this emission peak has a fine structure associated with shake-up processes (Fig. 3c), which are typical of Ni (II) compounds.[21] The BE for the Li 1s emission peak is located at 55.2 eV and appears as a broad signal. This value is close to that reported for Li_2O[22] and suggests, as expected, thorough ionization of Li atoms in the spinels.

All O 1s spectra exhibit complex profiles formed by a major component centered at 528.3–529.3 eV and attributed to Mn(M)–O–Mn(M) bonds. A second component, at 530.6–531.2 eV, is indicative of the presence of some additional oxygen compound, probably in the form of carbonate groups at particle surfaces. In fact, the C 1s signals exhibit two peaks: a stronger one located at 284.8 eV belonging to adventitious and a weaker one potentially accounting for the presence of surface carbonates. Moreover, the Fe 900 spinel possesses a third component of higher BE (532.4 eV) (see Fig. 3d). We tentatively assigned this component to Fe–OH acid groups formed at the surface of Fe_2O_3 particles.[18]

The structural characterization of the spinels was undertaken by Rietveld refinement of the XRD data,[23] using the GSAS software suite.[24] This analysis was performed by taking into account the following considerations: since the reduced intensity of the (220) reflections and increased intensity of the (111) reflections are consistent with the predominance of a normal spinel structure, with Li at 8a tetrahedral positions. Owing to the similarity of the X-ray scattering factors for Mn, Fe, Co and Ni, these ions cannot be distinguished with X-ray laboratory powder data. From crystal field arguments, Co^{3+} and Ni^{2+} have a strong tendency to occupy octahedral positions, so these cations must occupy 16d octahedral positions. Based on the crystal field theory, Fe^{3+} (high spin) exhibits no special preference for octahedral or tetrahedral positions. Based on its covalent bonding character, however, tetrahedral coordination should be preferred. The conditions used in the X-ray refinement of the spinel phases are summarized in Table 3 and the results obtained in Table 4. The composition data obtained, together with the lattice parameters, are listed in Table 5. Some results are worth special comment. Firstly, the compositions derived from the XRD data are in good agreement with those obtained from titration measurements (taking into account the errors inherent in chemical analysis and the presence of other phases as impurities). Secondly, there is a clear evidence that 8a sites are occupied by a small fraction of the transition elements.

Table 3 Conditions used in the refinement of X-ray data. Space group *Fd3m*[a]

Atom	Fraction	x[d]	y[d]	z[d]
Li[b]	Variable	1/8	1/8	1/8
M[b]	Variable	1/8	1/8	1/8
Mn[c]	Fixed	1/2	1/2	1/2
M[c]	Fixed	1/2	1/2	1/2
O	1	x[e]	x[e]	x[e]

[a]U_{iso}, 0.003 Å^2. [b]Assuming total occupancy of 8a by both ions. [c]Values fixed by the stoichiometry. [d]Coordinates. [e]x is approximately 0.26 depending on the sample composition.

Table 4 Refined parameters for the different spinels

Sample	R_{wp}[a]	R_p[a]	R_F[a]	o. f. (Li)[b]	x	o. f. (M)[b]
Fe 600	9.9	7.6	2.1	0.916(5)	0.2557(4)	0.170
Fe 900	15.4	11.8	5.3	0.858(6)	0.2537(4)	0.175
Co 600	8.0	6.1	1.9	0.908(6)	0.2550(4)	0.150
Co 900	10.4	7.6	3.3	0.913(5)	0.2586(3)	0.155
Ni 600	10.9	8.0	2.9	0.915(6)	0.2558(4)	0.160
Ni 900	11.9	8.9	5.2	0.916(5)	0.2557(4)	0.170

[a]*R*-factors (%): weighted pattern *R*-factor (R_{wp}); pattern *R*-factor (R_p); *R*-factor based on structure factors, F_{hkl}, (R_F). [b]Occupancy.

Table 5 Cation distributions and lattice parameters for the spinels as derived from X-ray data

Sample	Composition	a/Å
Fe 600	$[Li_{0.906}Fe_{0.094}]_{8a}[Mn_{1.77}Fe_{0.23}]_{16d}O_4$	8.2495(5)
Fe 900	$[Li_{0.856}Fe_{0.144}]_{8a}[Mn_{1.79}Fe_{0.21}]_{16d}O_4$	8.2691(4)
Co 600	$[Li_{0.908}Mn_{0.092}]_{8a}[Mn_{1.70}Co_{0.30}]_{16d}O_4$	8.1547(6)
Co 900	$[Li_{0.913}Mn_{0.087}]_{8a}[Mn_{1.69}Co_{0.31}]_{16d}O_4$	8.2010(2)
Ni 600	$[Li_{0.915}Mn_{0.085}]_{8a}[Mn_{1.68}Ni_{0.32}]_{16d}O_4$	8.1680(6)
Ni 900	$[Li_{0.915}Mn_{0.084}]_{8a}[Mn_{1.66}Ni_{0.34}]_{16d}O_4$	8.1900(3)

In some compounds, this results in a slight deficiency in Li ions relative to the composition established by chemical analysis. However, resolving this discrepancy is beyond the capabilities of the used method. Only a combined refinement of X-ray and neutron diffraction data can clarify the presence of Li/M vacancies at 8a sites. Thirdly, the Fe 900 sample exhibits two distinct, important features that are worth pointing out. It possesses a higher transition metal content at 8a sites; also, its X-ray peaks are broader than in the other two spinels obtained at 900 °C, thus suggesting lower particle crystallinity (*viz.* higher disorder in the cation arrangement). The lattice parameters are roughly consistent with the ionic radii of the doping elements; however, markedly greater dimensions for the Fe-based spinels—otherwise nearly coincident with those recently found by Ohzuku *et al.*[25] in $LiFe_yMn_{2-y}O_4$—are somewhat striking. Finally, the increased dimensions at high temperatures may reflect a decrease in the average Mn oxidation state (see Table 1) and a subsequent increase in Mn^{3+} at the expense of a decrease in the Mn^{4+} content on heating.

Electrochemical properties

Fig. 4 shows the first galvanostatic charge–discharge curves for the three spinels obtained at 400 °C and recorded over the 5.2–3.5 V range. Lithium extraction essentially occurs in two steps of different charge depth. The low voltage step for Fe- and Co-doped spinels amounts to 66 and 37 A h kg^{-1}, whereas that for Ni spinel is as high as 150 A h kg^{-1}. The trend in the capacity values of the high voltage step is reversed; thus, that for the Ni spinel is only 72 A h kg^{-1}. For all three compounds at 5.2 V, the cells are overcharged by about 50% and deliver only less

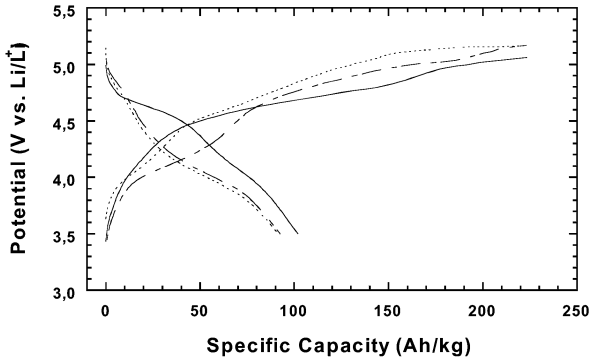

Fig. 4 Charge–discharge curves for the cells made from spinels calcined at 400 °C; (···) Fe, (· – ·) Co and (—) Ni.

than 46% of the charge received. The strong polarization of the discharge curves and their shape differences from the respective charge curves reflect the irreversibility of the lithium extraction/insertion processes, the origin of which may be the poor crystallinity of the spinels. In fact, the spinel framework collapses and the material becomes virtually amorphous upon Li extraction. Particle surface roughness may reasonably facilitate decomposition of the electrolyte at so high voltages, which may account for the high overcharge observed.

Fig. 5 shows the voltage profiles for different $Li/LiM_xMn_{2-x}O_4$ cells made from spinels obtained at 600 °C in the first, fifth and twentieth cycle over the 3.5–5.2 V range. The potential–capacity curves, like those for the 400 °C spinels, exhibit significant differences in shape and hence in the capacity associated with the different redox reactions involved. Thus, in the first charge process, the Co 600 sample exhibits two well-defined plateaux of similar length at 4.1 and 5.1 V. These two steps are clearly observed in the subsequent discharge process. The Ni 600 sample exhibits a pronounced plateau at 4.8 V and a barely distinguishable one at 4.1 V. By contrast, the Fe 600 sample exhibits an extended plateau at 4.2 V and a decreased plateau at 5.1 V. This material exhibits a somewhat peculiar

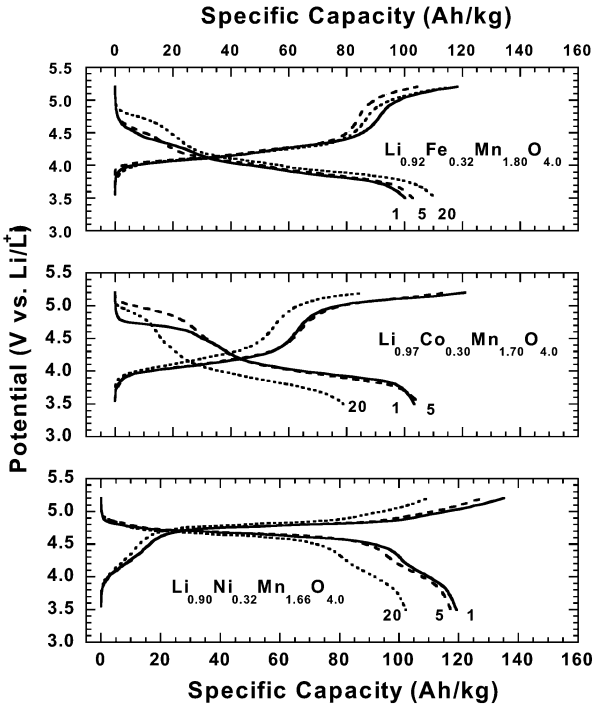

Fig. 5 Charge–discharge curves for Li/Li–M–Mn–O cells cycled over the voltage range 3.5–5.2 V. Spinels prepared at 600 °C. Numbers indicate first, fifth and twentieth cycles.

behavior in the reverse reaction, particularly that responsible for the higher voltage step, which reflects in a plateau in the discharge curve that increases in length with cycling. Table 6 summarizes the capacity values for some cycles. The theoretical capacity was estimated by assuming the voltage plateau centered at *ca.* 4.2 V to be due to the redox reaction $Mn^{3+}\leftrightarrow Mn^{4+}$, and that at the higher voltage to result from a redox reaction affecting the doping metal (*viz.* $Fe^{3+}\leftrightarrow Fe^{4+}$; $Co^{3+}\leftrightarrow Co^{4+}$; $Ni^{2+}\leftrightarrow Ni^{4+}$). These latter reactions of Co and Ni were recently documented from X-ray fine-structure absorption measurements,[26] and the former by Mossbauer spectroscopy.[25,27] The total capacity in the 3.5–5.2 V region was calculated by assuming lithium to be thoroughly removed from the structure.

The Ni 600 spinel is the only one that has an overall delivered capacity similar to that expected from theoretical calculations. However, the capacity delivered by the oxidation of Ni^{2+} to Ni^{4+} is nearly 25% greater than the theoretical one, whereas the opposite is true for the capacity delivered by the Mn^{3+} oxidation. The origin of these anomalous capacities is unclear; however, unexpected capacity values have also been found in other Ni-containing spinels (*e.g.* $LiNi_{0.5}Mn_{1.5}O_4$).[7,9] This material exhibits a *pseudo* plateau at about 4.2 V which accounts for about 12–15 A h kg^{-1} in spite of the absence of Mn^{3+}. Cell capacity fades slowly upon successive cycling (similarly to $LiNi_{0.5}Mn_{1.5}O_4$ as found by Ein-Eli *et al.*[7]), also, the material retains 78% of the initial value after 50 cycles, but preserves a satisfactory coulombic efficiency.

The Co 600 sample delivers only 83% of its theoretical capacity, the capacity loss being more severe in the higher voltage reaction. In fact, the capacity of the 5 V step is somewhat greater than that derived from the Co^{3+} content. Assuming other cobalt species such as Co^{2+} to be the origin of this divergence would be inconsistent with the XPS data and thermodynamic considerations. Side reactions (*e.g.* the electrolyte oxidation potentially occurring at such high voltages) might result in an overestimated cell capacity. Cycling properties are worse than those of the Ni-doped spinel as the cell retains only about 58% of its initial capacity after 50 cycles. This decreased capacity affects the higher voltage reaction preferentially. This spinel performs similarly to that recently reported by Kawai *et al.*,[11] for a spinel of nominal composition $LiCoMnO_4$, which, based on extrapolation of reported data, retained about 54% of its initial capacity after 50 cycles.

The capacity of the Fe 600 spinel is lower than that calculated for the two steps. Although the initial capacity of the charging process is lower than that reported by Kawai *et al.*[5] for a spinel of nominal composition $LiFe_{0.5}Mn_{1.5}O_4$ (140 *vs.* 117 A h kg^{-1}), our spinel exhibits superior cycling properties and retains 90% of its initial cell capacity after 50 cycles compared to only 54% in $LiFe_{0.5}Mn_{1.5}O_4$ after 36 cycles. Moreover, capacity fading above the 20th cycle affects the 3.5–4.5 V plateau mainly,

Table 6 Specific capacities (A h kg^{-1}) for the charging of Li/Li–M–Mn–O cells. Roman numbers indicate cycle numbers. Values in brackets are theoretical capacities

Sample	3.5–4.5 V	4.5–5.2 V	3.5–5.2 V
Fe 600	I → 85 (154)	I → 32 (45)	I → 117 (131)
	V → 80	V → 23	V → 103
	XX → 82	XX → 32	XX → 114
	L → 74	L → 30	L → 104
Co 600	I → 59 (100)	I → 61 (45)	I → 120 (143)
	V → 61	V → 53	V → 114
	XX → 52	XX → 34	XX → 86
	L → 42	L → 28	L → 70
Ni 600	I → 17 (26)	I → 118 (95)	I → 135 (133)
	V → 16	V → 111	V → 127
	XX → 13	XX → 96	XX → 109
	L → 12	L → 86	L → 98

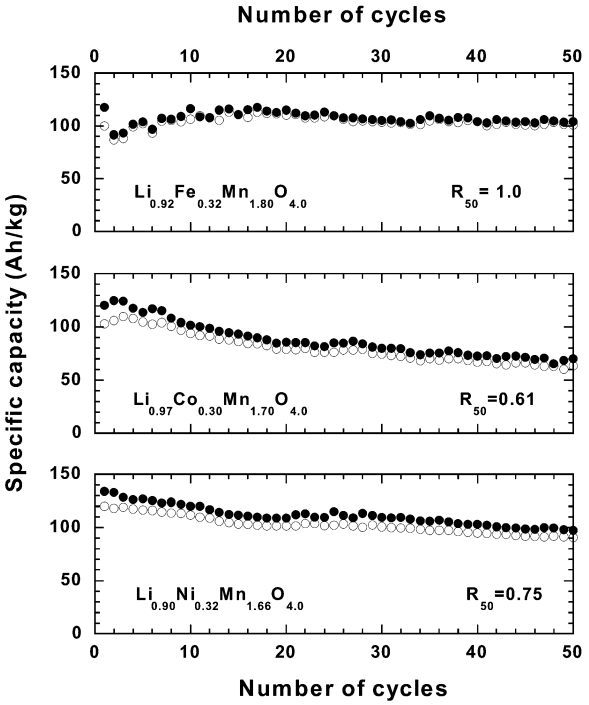

Fig. 6 Variation of the specific capacity of Li/Li–M–Mn–O cells cycled over the voltage range 3.5–5.2 V. Spinels prepared at 600 °C.

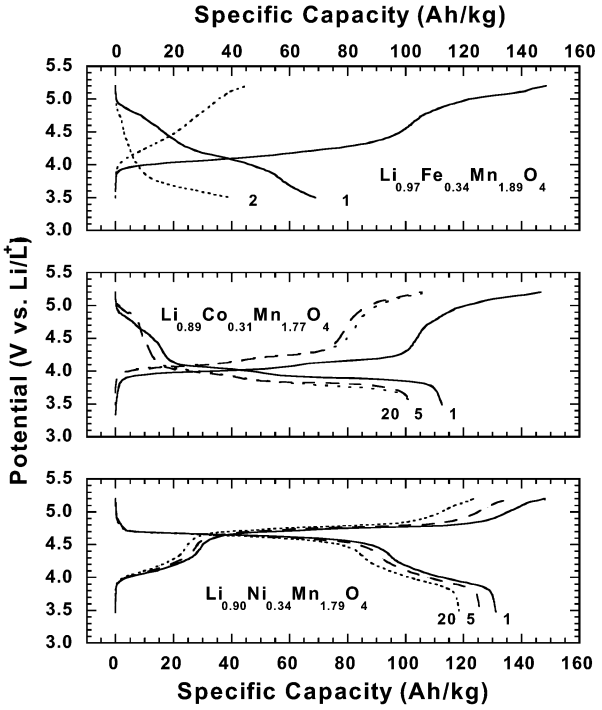

Fig. 7 Charge–discharge curves for Li/Li–M–Mn–O cells cycled over the voltage range 3.5–5.2 V. Spinels prepared at 900 °C. Numbers indicate first, fifth and twentieth cycles.

whereas the capacity observed in the high voltage region remains virtually constant on cycling.

Fig. 6 shows the variation of the delivered charge–discharge capacity as a function of the number of cycles. For easier comparison, we have included the R_{50} factor, defined as the ratio between the specific capacities delivered in the fiftieth and first cycles. As can be seen, cycling performance in the Ni- and, particularly, the Co-doped spinel, gradually declines; on the other hand, the Fe-doped spinel exhibits excellent capacity retention during cycling. Furthermore, this spinel exhibits the smallest difference between charge and discharge capacity and thus possesses better coulombic efficiency than the cells based on Co- and Ni-containing electrodes. It is worth noting that the largest differences in charge–discharge values for the latter two electrodes are observed in the first few cycles. This is consistent with decomposition of the electrolyte in the high voltage region, to a lesser extent than in the samples prepared at 400 °C, as a result of a smoother particle surface (see Fig. 2B). As the number of cycles increases, the formation of a protective thin film on the active particle surface may stabilize the electrolyte. In fact, the delivered capacities obtained after the first five cycles are consistent with the chemical composition of the electrode. By contrast, Fe-doped particles seem to be less active towards electrolyte decomposition in spite of their ability to yield 5 V redox reactions.

Fig. 7 shows the voltage profiles for the Li cells made from the three spinels prepared at 900 °C at different cycling stages. The main resemblance between the first charge profiles and those belonging to the samples calcined at 600 °C (Fig. 5) is the preservation of the two plateaux at similar voltages and associated with the above-mentioned oxidation processes undergone by Mn^{3+} and the substituting transition metal M^{n+}. In fact, these data provide indirect evidence for the presence of Fe^{3+} in the spinel framework and that only a portion of this cation leaves the structure to form α-Fe_2O_3. However, the capacity of the low-voltage step centered at *ca.* 4.2 V is higher, particularly in the Co and Ni samples. This should be consistent with the decrease in the average Mn oxidation state obtained by titration, which must result in an increased Mn^{3+} content. Table 7 shows the experimental and theoretical capacity values. The peculiar behavior of the Ni-based spinel (*viz.* a reduced capacity of the low plateau and a capacity greater than the theoretical one corresponding to the Ni^{2+} oxidation), is maintained. The overall capacity of the first charge in the Co-doped sample increases significantly and, as in the Ni-containing spinel, is somewhat greater than that derived from the chemical composition. However, the most salient difference from the samples prepared at 600 °C is exhibited by the Fe 900 sample, the capacity of which fades abruptly on cycling. For this reason, it was excluded from Table 7. Collapse of the spinel framework as the origin of this unexpected behavior can be discarded. The XRD patterns for the cathodes charged at 5.2 V, Fig. 8, reveal that the three compounds preserve the main peaks for the spinel structure. However, the quality of these spectra is quite poor owing to a significantly decreased signal-to-noise ratio. This precludes further analysis of these X-ray data. In our opinion, a number of subtle factors act in combination to hinder the lithium insertion reaction in the Fe 900 sample. One such factor is the high transition metal content at the 8a sites relative to the Co and Ni spinels (Table 5). In fact, the XRD pattern for the oxidized Fe spinel at 5.2 V, Fig. 8 (top pattern), exhibits a weak reflection at 2.84 Å due to the (220) plane. This reflection, which accounts for the presence of transition metal cations (probably iron ions) at the 8a sites, is hardly discernible in the other two spinels. This means that the cation distribution in the Fe 900 spinel remains virtually unaltered upon lithium extraction. Since Li ions must be accommodated at the vacant tetrahedral sites in the

Table 7 Specific capacity (A h kg^{-1}) for the charging of Li/Li–M–Mn–O cells. Roman numbers indicate cycle numbers. Values in brackets are theoretical capacities

Sample	3.5–4.5 V	4.5–5.2 V	3.5–5.2 V
Co 900	I → 103 (130)	I → 42 (46)	I → 139 (135)
	V → 77	V → 26	V → 103
	XX → 78	XX → 25	XX → 103
Ni 900	I → 37 (103)	I → 123 (100)	I → 140 (133)
	V → 27	V → 105	V → 132
	XX → 24	XX → 96	XX →120

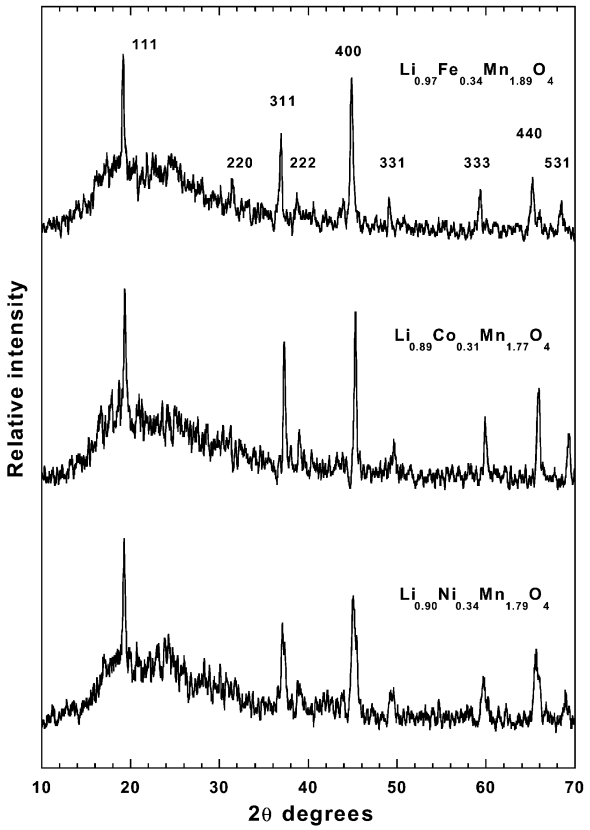

Fig. 8 XRD patterns for the spinels prepared at 900 °C and charged to 5.2 V.

discharge process, the presence of highly charged cations partly occupying these positions should act as a barrier against Li insertion. One other factor is related mainly with the textural and morphological properties of the particles. Whereas the Co and Ni spinels prepared at 900 °C consist of particles highly uniform in size, most of them adopting a regular *pseudo* octahedral shape, Fig. 2C, the Fe 900 spinel particles are larger and less uniform in size and morphology (Fig. 2D).

Fig. 9 shows the variation of charge–discharge capacity for the Co 900 and Ni 900 spinels as a function of the number of cycles. A comparison of these data with those for the Co 600 and Ni 600 samples (Fig. 7) clearly reveals that cycling performance improves on heating at higher temperatures.

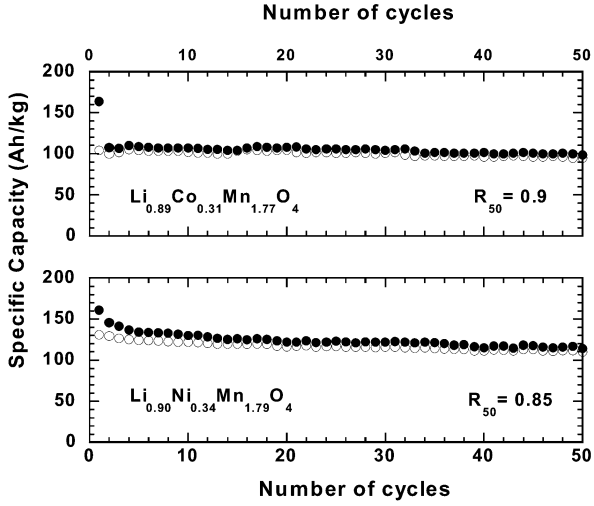

Fig. 9 Variation of the specific capacity of Li/Li–M–Mn–O cells cycled over the voltage range 3.5–5.2 V. Spinels prepared at 900 °C.

The coulombic efficiency of the two cells is close to unity; also, they exhibit an excellent capacity retention on cycling. Apparently, the electrolyte decomposition after the first few cycles seems to cease and the charge–discharge capacity remains remarkably constant on successive cycles. It is highly illustrative how differences in the synthetic conditions can affect the factors governing cell performance. Thus, the cell made from a spinel of nominal composition $LiNi_{0.5}Mn_{1.5}O_4$ reported by Ein-Eli *et al.*[7] and cycled at the same current density as ours exhibits a larger difference in capacity between the charge and discharge cycles. Also, its discharge capacity fades slowly from 120 to 86 A h kg^{-1}. The proposed explanation assumes decomposition of the electrolyte. Because this spinel was prepared at 750 °C, its particle surface morphology may be the origin of its poor electrochemical properties. On the other hand, the improved crystallinity and particle morphology of the Co- and Ni- containing spinels may be the origin of their attractive electrochemical behavior.

Conclusions

Spinels of nominal composition $LiM_xMn_{2-x}O_4$ (M = Fe, Co, Ni; $x \approx 0.3$) were tested as positive electrodes in lithium cells operating at high voltage values (3.5 to 5.2 V) and, although all the spinels adopt a cubic structure, they exhibit differences in electrochemical behavior. Thus, the series obtained at 400 °C exhibits poor reversibility towards lithium extraction/insertion; also, discharge capacity fades abruptly after the first charging process. Decreased crystallinity and significant particle surface roughness, which can result in oxidation of the electrolyte at such high voltages, are the main reasons for the capacity loss. The higher crystallinity and smoother particle surfaces at higher temperatures result in better electrochemical performance of the lithium cells. In fact, the cells made from Co900 and Ni 900 spinels exhibit excellent capacity retention upon extensive cycling. However, the Fe 900 spinel performs worse than the Fe 600 spinel (the discharge capacity of the cell drops abruptly over the first few cycles). This anomalous behavior may be due to the differences found in textural and structural properties. These results reflect the difficulty in optimizing doped Li–Mn spinels acting as 5 V electrodes, as subtle differences that are difficult to control can have dramatic effects on their electrochemical behavior. Under the synthetic conditions used in this study, this difficulty was only encountered with the Fe-containing spinel, an otherwise inexpensive, environmentally friendly element.

Acknowledgement

This work was supported by Junta de Andalucía (Group FQM-175).

References

1 G. T. Fey, W. Li and J. R. Dahn, *J. Electrochem. Soc.*, 1994, **141**, 2279.
2 C. Sigala, D. Guyomard, A. Verbaere, Y. Piffard and M. Tournoux, *Solid State Ionics*, 1995, **81**, 167.
3 C. Sigala, A. Verbaere, J. L. Mansot, D. Guyomard, Y. Piffard and M. Tournoux, *J. Solid State Chem.*, 1997, **132**, 372.
4 L. Hernán, J. Morales, L. Sánchez, J. Santos and E. Rodríguez Castellón, *Solid State Ionics*, 2000, **133**, 179.
5 H. Kawai, M. Nagata, M. Tabuchi, H. Tukamoto and A. R. West, *Chem. Mater.*, 1998, **10**, 3266.
6 H. Kawai, M. Nagata, H. Tukamoto and A. R. West, *Electrochem. Solid State Lett.*, 1998, **1**, 212.
7 Y. Ein-Eli, J. T. Vaughey, M. M. Thackeray, S. Mukerjee, X. Q. Yang and J. McBreen, *J. Electrochem. Soc.*, 1999, **146**, 908.
8 Y. Ein-Eli, F. Howard Jr, S. H. Lu, S. Mukerjee, J. Mc Breen, J. T. Vaughey and M. M. Thackeray, *J. Electrochem. Soc.*, 1998, **145**, 1238.

9 T. Ohzuku, S. Takeda and M. Iwanaga, *J. Power Sources*, 1999, **81–82**, 90.
10 S. Panero, D. Satolli, M. Salomon and B. Scrosati, *Electrochem. Commun.*, 2000, **2**, 810.
11 H. Kawai, M. Nagata, H. Kageyama, H. Tukamoto and A. R. West, *Electrochim. Acta*, 1999, **45**, 315.
12 L. Sánchez and J. L. Tirado, *J. Electrochem. Soc.*, 1997, **144**, 1939.
13 J. Morales, L. Sánchez and J. L. Tirado, *J. Solid State Electrochem.*, 1998, **2**, 420.
14 D. Briggs and M. P. Seach, in *Practical Surface Analysis*, John Wiley & Sons, Chichester, 1990, vol. 1, p. 598.
15 C. D. Wagner, W. M. Riggs, L. E. Davis, J. F. Moulder and G. E. Mullenberg, in: *Handbook of X-ray Photoelectron Spectroscopy*, Perkin-Elmer Corporation, Physical Electronic Division, Eden Prairie, MN, 1979.
16 M. Langlet, A. D'Huysser, J. Kasperek, J. P. Bonnelle and J. Durr, *Mat. Res. Bull.*, 1985, **20**, 745.
17 C. D. Wagner, *Faraday Discuss. Chem. Soc.*, 1975, **60**, 291.
18 N. S. McIntyre and D. G. Zetaruk, *Anal. Chem.*, 1977, **49**, 1521.
19 L. Armelao, R. Bertoncelli, L. Crociani, G. Depaoli, G. Granozzi, E. Tondello and M. Bettinelli, *J. Mater. Chem.*, 1995, **5**, 79.
20 K. Amine, H. Tukamoto, H. Yasuda and Y. Fujita, *J. Electrochem. Soc.*, 1996, **143**, 1607.
21 A. E. Bocquet, T. Mizokawa, T. Saitoh, H. Namatame and A. Fujimori, *Phys. Rev. B*, 1992, **46**, 3777.
22 K. Kanamura, H. Tamura, S. Shiraishi and J. Takehara, *J. Electrochem. Soc.*, 1995, **142**, 340.
23 H. M. Rietveld, *J. Appl. Crystallogr.*, 1969, **2**, 65.
24 A. C. Larson and R. B. Von Dreele, *Los Alamos National Lab. Rep. No. LA-UR-86-748*, 1994.
25 T. Ohzuku, K. Ariyoshi, S. Takeda and Y. Sakai, *Electrochim. Acta*, 2001, **46**, 2327.
26 Y. Terada, K. Yasaka, F. Nishikawa, T. Konishi, M. Yoshio and I. Nakai, *J. Solid State Chem.*, 2001, **156**, 286.
27 H. Shigemura, H. Sakaebe, H. Kageyama, H. Kobayashi, A. R. West, R. Kanno, S. Morimoto, S. Nasu and M. Tabuchi, *J. Electrochem. Soc.*, 2001, **148**, A730.